Biomolecules and Biomedicine
ISSN: 2831-0896 (Print) | ISSN: 2831-090X (Online)

Journal Impact Factor® (2023): 3.1
CiteScore®(2023):7.4
www.biomolbiomed.com | www.blog.bjbms.org

RESEARCH ARTICLE

Nong et al: PJ34 inhibits parthanatos in hair cells

PJ34 prevents cisplatin-induced hair cell loss via inhibition of PARP-1–AIF parthanatos

Huiming Nong[1], Xiru Zhang[2], Yingxue Yuan[2], Junhong Zhang[1], Jingyi Zhao[2], Zhixin Cao[2*]

[1]Department of Otolaryngology, Shandong Provincial Hospital Affiliated to Shandong First Medical University, Shandong Province, China

[2]Department of Pathology, Shandong Provincial Hospital Affiliated to Shandong First Medical University, Shandong Province, China.

*Correspondence to **Zhinxin Cao**: caozhixin12@126.com

DOI: https://doi.org/10.17305/bb.2025.12533

ABSTRACT

The poly (ADP-ribose) polymerase-1 (PARP-1) inhibitor PJ34 acts as an anti-inflammatory and neuroprotective agent by modulating parthanatos. This study aimed to explore the protective effects of PJ34 against cisplatin-induced injury in auditory cells and to elucidate its underlying mechanism of action. Flow cytometry and immunofluorescence were employed to detect apoptosis in HEI-OC1 and ovarian cancer cell lines. Additionally, immunofluorescence and Western blotting were used to assess changes in the expression of related proteins, including cleaved Caspase-3, PARP-1, and cytosolic apoptosis-inducing factor (AIF), across the groups. Mitochondrial membrane potential (MMP) levels were measured using the MMP assays, and reactive oxygen species (ROS) levels were assessed by MitoSox red staining. Our results indicate that treatment with 30 μM cisplatin activates cleaved Caspase-3, promotes PARP-1 overexpression, and facilitates AIF nuclear translocation, leading to decreased MMP and increased ROS accumulation, which ultimately triggers auditory cell death. Treatment with 2.5 μM PJ34 mitigated PARP-1 overexpression and AIF nuclear translocation following cisplatin exposure, reduced the decline in MMP, and decreased ROS accumulation, thereby alleviating damage to auditory cells. Conversely, PJ34 enhanced the damaging effects of cisplatin on ovarian cancer cell lines. In conclusion, our findings suggest that PJ34 may reduce cisplatin-induced hair cell death by regulating PARP-1-mediated parthanatos. Notably, PJ34 shows promise as a potential novel therapeutic agent for the prevention and/or treatment of cisplatin-induced ototoxicity.

Keywords: Hair cells; hearing loss; cisplatin; PARP inhibitor; AIF; parthanatos.

INTRODUCTION

Poly (ADP-Ribose) polymerase-1 (PARP-1) is a 116 kDa multifunctional nuclear protease that can regulate a variety of biological functions [1]. As a group of enzymes responsible for DNA damage monitoring and repair, PARP-1 is activated when cellular DNA is damaged, initiating the DNA repair mechanism by PARylation. Interestingly, the degree to which PARP-1 is activated is dependent upon the extent of DNA lesions. Hyperactivation of PARP-1 can cause nuclear translocation of the apoptosis inducing factor (AIF), which, in turn, triggers parthanatos contributing to cell death [2].

In many pathological situations, oxidative-dependent damage leads to massive DNA breaks, PARP-1 is hyperactivated, and the nucleus produces and releases toxic levels for poly (ADP-ribose) (PAR) into the plasma, where PAR binds to mitochondrial membrane proteins, leading to increased mitochondrial membrane permeability and depolarization, which facilitates the mitochondrial release of AIF into the cytoplasm. AIF in the cytoplasm binds to macrophage migration inhibitory factor (MIF) and enters the nucleus, leading to chromatin and DNA breaks that trigger a PARP-1-mediated cell death program[3, 4]. Relevant studies have demonstrated that PARP-1 inhibitor (PARPi) PJ34 can block PARP-1 binding to Nicotinamide adenine dinucleotide (NAD+) through a competitive inhibition mechanism, which prevents the overconsumption of NAD+ and reduces the depletion of the cellular energy pool, thereby alleviating the metabolic disorders of the cells and the subsequent cell death [5, 6]. In recent years, studies have shown that the PJ34 may exert an intestinal mucosal structure protective effect in mice with acute colitis and neuroprotective effects after traumatic brain injury [1, 7]. Furthermore, numerous studies have shown that PARP-1 expression is over-regulated in cancer cell lines [8, 9]. Inhibiting PARP-1 causes a decrease in DNA repair function and is considered to be an important mechanism to alleviate cisplatin resistance in

cancer cells [10]. It has been shown that PJ34 can increase sensitivity to cisplatin therapy in non-small cell lung carcinoma (NSCLC) cellular models through increasing the accumulation of platinum adducts[11]. Furthermore, PJ34 can also coordinate with gemcitabine and cisplatin to mediate more cancer cell death in triple-negative breast cancer cells [12]. Many studies have shown that PARPi not only exert synergistic anticancer effects together with cisplatin, but also exert anti-cisplatin nephrotoxicity effects. It has been reported that pharmacological inhibition or genetic ablation of PARP-1 in murine models of cisplatin-mediated nephrotoxicity can reduce renal histopathological damage, which attenuated cisplatin-induced nephrotoxicity[13]. The union of PJ34 and 3-aminobenzamide ameliorates renal function as well as histological damage in zebrafish and mouse models of cisplatin nephrotoxicity [14]. Considering the variability of the co-action of PJ34 and cisplatin under different pathophysiologies, the experimental design of the influence of PJ34 on ototoxicity induced by cisplatin is one of the rational approaches to study. Indeed, it has been shown in a number of studies that suppression of PARP-1 is considered to be a useful strategies to attenuate cisplatin ototoxicity. It has been suggested that overexpression of PARP-1 takes a key role in cisplatin-induced damage to cochlear tissues and HEI-OC1 cells, and that suppression of PARP-1 activation attenuates ototoxicity by restoring cisplatin-induced decreases in ATP and NAD+ levels[15]. Another study indicated that inhibition of PARP-1 expression and reduction of nucleotranslocation of AIF could attenuate cisplatin-induced vascular stria damage, thereby reducing hearing loss [16]. In addition, inhibition of PARP-1 expression can also reduce the decreased hearing loss induced by streptozotocin and noise [17, 18]. Taken together, PARP-1 is thought to be a possible key target the treatment of impaired hearing.

Cisplatin, a platinum-based chemotherapeutic agent, remains a cornerstone in the clinical management of diverse human malignancies. However, the use of cisplatin has been severely limited due to its serious side effects, including nephrotoxicity and ototoxicity [19, 20]. Hearing loss of varying degrees has been reported in about 40-60%

of patients treated with cisplatin, with 18% developing severe to profound hearing loss [21]. The mechanism by which cisplatin causes hearing loss is not fully understood, and current studies consider it to be primarily attributable to increased ROS and mitochondrial dysfunction [21, 22]. It has been shown that increased mitochondrial ROS levels after cisplatin exposure act as an initiator to decrease MMP, inducing the mitochondrial apoptotic pathway mediated by Bcl-2 and cleaved caspase-3 which results in irreversible auditory cell death [23]. In addition, it has been reported that cisplatin induces cochlear vascular stria damage in mice through activation of cleaved caspase-3, PARP-1 , as well as promotion of nuclear translocation of AIF , which leads to severe ototoxicity [16]. Until now, there have been no reports examining the influence of PJ34 on cochlear hair cells （HCs） damage induced by cisplatin. Therefore, we investigated whether PJ34 could attenuate cisplatin-treated mouse HCs and HEI-OC1 cell line injury, with a special focus on changes in PARP-1 and AIF expression, as well as the dynamics of the mitochondrial apoptotic pathway and mitochondrial function. Furthermore, we used the same concentration of PJ34 and cisplatin co-treated in tumor cell lines to explore the potential of PJ34 to attenuate cisplatin ototoxicity without attenuating the tumoricidal effect of cisplatin in tumor cell lines. To determine the effect of PJ34 on the anti-cancer effects exerted by cisplatin, we examined the apoptotic rate of ovarian cancer cell TOV112D and HEY cell lines at different concentrations of PJ34 and 30 μM cisplatin using flow cytometry. Once confirmed, it is very encouraging that PJ34 will be regarded as a potent pharmacological candidate for ameliorating cisplatin-induced ototoxicity, and become the first drug to obtain the desired tumor-killing effect while reducing the adverse effects of cisplatin ototoxicity and nephrotoxicity.

MATERIALS AND METHODS

Animals and treatments

This study utilized C57BL/6 mice, aged 3 days postpartum (P3). The mice were

procured through an ISO-certified supplier (Spelford Biotechnology Co., Beijing, China) for experimental implementation. As AVMA (American Veterinary Medical Association) states, physical methods (e.g., cervical dislocations, rapid amputations) are permissible for rodent pups ≤7 days old without anesthesia due to their immature nociceptive pathways. In this experiment, we used a pre-checked WPI mouse guillotine. P3 mice were gently grasped, manually immobilized, head positioned in the guillotine slot, and decapitated in one attempt to ensure rapid cerebral blood supply interruption and unconsciousness. Death was confirmed by absent heartbeat, respiration, and pupillary reflexes. Operator Huiming Nong is experienced and trained. The study was approved by the Animal Protection Committee of Shandong Provincial Hospital (Approval No. ECAESDUSM 20123011). Additionally, we also referred to the protocols for euthanasia of experimental animals by Herling, A.W. (2016) [24]and Kumar, M. (2017)[25].

Cell line and cell culture

The HEI-OC1 auditory progenitor cell line (RRID: CVCL-D899, KMCC-001-1439, Coweldgen Scientific Co.,LTD, CN), an in vitro model exhibiting phenotypic characteristics reminiscent of cochlear hair cells and originating from murine organ of Corti explants, were maintained in DMEM-high glucose formulation (C11995500BT, Gibco, USA) supplemented with 10% (v/v) fetal bovine serum (FBS, 16000-044, Gibco, USA) in antibiotic-free culture conditions, following standardized culture protocols (33±0.5°C, 5% CO_2, 95% humidity) for experimental implementation.

HEY cell lines (RRID: CVCL-0671, CL-0671, Pricella, CN), were cultured in HEY medium (CM-0671, Pricella, CN). TOV112D cell lines (RRID: CVCL-3612, FH1271, FuHeng Biology, CN), were cultured in TOV112D medium (FH-TOV-112D, FuHeng Biology, CN). HEY and TOV112D cell lines were cultured under permissive conditions (37 ℃, 5% CO_2).

The HEI-OC1 cell line was identified by Real-time Quantitative PCR Detecting System (QPCR), HEY cell line and TOV112D cell line were identified by Short Tandem Repeat (STR). The above cell lines tested negative for mycoplasma.

Cochlear explants culture and treatment

P3 C57BL/6 mice were severed from their heads and dissected along the middle cranial suture to expose the bilateral temporal bones, and the cochlea was carefully removed under a microscope. The whole basement membrane was dissected out and laid flat on a 10 mm thick slide pre-coated with Cell-Tak adhesive. The organs were maintained in Gibco™ DMEM/F12 Basal Medium (1056018, Gibco, USA) supplemented with a defined cocktail of B-27™ Serum-Free Supplement (17504044, Gibco, USA), N-2™ Supplement (17502048, Gibco, USA), and ampicillin sodium salt (A1170, Solarbio, China) at 37 ± 0.5°C in a humidified incubator equilibrated with 5% CO_2/95% air within a sterility-validated culture system.

Drug treatments

Building upon our prior research utilizing cisplatin (P4394, Sigma-Aldrich, USA) at 30 μM concentration for 24-hour exposure periods [26], this study implemented a standardized cisplatin dosing protocol (24 hours /30 μM) while investigating synergistic effects with PJ34 (HY-13688A, MedChemExpress, USA). Experimental groups included a cisplatin monotherapy cohort administered at established optimal parameters, and a combinatorial treatment group receiving 2.5 μM PJ34 for 24 hours concomitant with cisplatin.

Immunofluorescence staining

The original medium was removed and washed three times with pre-cooled PBS, 4% paraformaldehyde (PFA) was used to immobilize the cells, and Triton X-100s and PBS were mixed in order to be used to perforate the cells. The crawling sheet with adherent cells underwent sequential processing, including a 1-hour incubation in 1% Bovine

serum albumin (BSA) /PBS buffer (pH 7.4) at 22±1°C followed by overnight exposure to primary antibody cocktails at 4°C in a humidified chamber. The primary antibodies employed in this investigation consisted of anti-PARP-1 antibody (1:250, 13371-1-AP, Proteintech, CN), anti-AIF antibody (1:250, 17984-1-AP, Proteintech, CN), and anti-cleaved caspase-3 antibody (1:500, 9664 s, CST, US). After three PBS washes, the specimens were treated with secondary fluorescent antibodies and DAPI (d9542, Sigma-Aldrich, US) for 1 hour in darkness. Finally, the slides were mounted, and observations were made utilizing a Leica TCS SP8 confocal laser scanning microscope (Leica Microsystems, Germany) equipped with 405/488/552/647 nm laser lines and a 63× oil-immersion objective (NA 1.4). Each image shown is representative of a separate cochlear explant.

MitoSox red staining

After treatment, the cochlear explants underwent sequential processing involving three PBS buffer rinses (pH 7.4) at 37°C, followed by 10-minute incubation with MitoSox Red mitochondrial superoxide indicator (3 μM, ThermoFisher, USA) under light-protected conditions (22±1°C). Fluorescence detection was performed using a Leica TCS SP8 confocal fluorescence microscope (Leica Microsystems, Biberach, Germany).

Protein extraction and Western blot (WB)

Total proteins from variously processed cells and tissues were taken with RIPA lysate (R0020, Solarbio, CN) containing protease inhibitors (p0100, Solarbio, CN) and phosphatase inhibitors (HY-K0022, MCE, CN). Following centrifugation, the supernatant was collected, the total protein concentration was quantified using BCA (Bicinchoninic Acid) protein assay kit (pc0020, Solarbio, CN). Proteins were resolved via 10% sodium dodecyl sulfate-polyacrylamide gel electrophoresis (SDS-PAGE), followed by electrotransfer to polyvinylidene difluoride membranes (PVDF, pore size 0.45 μm, ISEQ00010, Merck Millipore, CN) for 90 minutes. Membrane blocking was performed using 5% (w/v) BSA or 5% (w/v) non-fat dry milk in TBST（Tris-buffered

saline with 0.1% Tween-20 ）for 1 hour at ambient temperature (22±1°C). The next day incubate with the corresponding diluted anti for 1 hour at ambient temperature. The final assay was performed using the ECL Kit (WBKLS0100, Millipore, US) and the results were analyzed using ImageJ software[27]. The primary antibodies used included anti-PARP-1 antibody (1:1000, 13371-1-AP, Proteintech, CN), anti-AIF antibody (1:1000, 17984-1-AP, Proteintech, CN), anti-cleaved caspase-3 antibody (1:1000, 9664 s, CST, US), and anti-GAPDH (1:5000, 60004–1-lg, Proteintech, CN).

Flow cytometry

Apoptosis incidence was quantified using the Annexin V/PI apoptosis detection kit (556547, BD Biosciences) followed by flow cytometric analysis on a FACS Calibur system (FACS, BD, US) with a total of 10,000 cells per group. Evaluation was conducted utilizing Flow Jo 10.8 software.

Co-localization analysis of AIF and DAPI

We measured the co-localization of AIF (red fluorescence) and DAPI (blue fluorescence) by Image J software. We surveyed the length of the scale bar (20 μm) in the figure, selected a typical cell, and drew a line running along the lengthwise axis of the cell using the “Line Segment” tool, and measured the fluorescence intensity on the line segment using the "Plot profile" tool. The horizontal coordinate is distance (μm), the length of the cell longitudinal axis, and the vertical coordinate is intensity arbitrary units (a.u.), the intensity of red fluorescence and blue fluorescence. The overlap of the AIF and DAPI curves in the coordinate axes indicates their co-localization.

Cytoplasmic and nuclear protein extraction

Cytoplasmic and nuclear protein fractions were isolated by the Nuclear and Cytoplasmic Protein Extraction Kit (P0027, Beyotime Biotechnology, Shanghai, China) following standardized protocols. Adherent cells were collected from six-well plates with PBS, centrifuged and the supernatant was discarded to obtain cell precipitates, and

then the precipitates were resuspended with 200 μl of Reagent A mixture containing 1 mM PMSF (P0100, Solarbio, CN). After chilling the cell suspension on ice for 15 min, 10 μl of Reagent B was added, and the cells were then centrifuged at 16,000 g at 4°C for 5 min. The resulting supernatant, comprising cytoplasmic proteins, was collected, precipitated, and then resuspended with 50 μl of nuclear protein extraction reagent containing 1 mM PMSF. After being vortexed and ice bath in turn for 30 min, the mixture was centrifugated and the supernatant was preserved as the nuclear protein.

Mitochondria membrane potential (MMP, Δψm)

MMP fluctuations were evaluated utilizing the Mitochondrial Membrane Potential Assay Kit with JC-1 (Beyotime). In short, the processed cells in six-well plates were gathered and subjected to two washes with cold PBS. The cells were incubated in 500 μl of culture medium and 500 μl of JC-1 working solution, protected from light at 37°C for 20 min. In healthy cells, MMP remains within the normal range , and JC-1 accumulates in the mitochondrial matrix to form J-aggregates that emit red fluorescence. However, when cells are in an unhealthy state, MMP is significantly reduced, resulting in the dissociation of JC-1 from mitochondria and its aggregation in the cytoplasm in uniporter form, which emits green fluorescence.

Cell counting

For the purpose of quantifying cells, we captured images of the cochlea using a 40 × 2.5 objective and used Image J software to quantify the immunostaining positive cells. Specifically, we calibrated the scale in Image J software to 40 μm based on the relative length of the scale bar (40 μm) in the figure. Subsequently, we measured the total length of the cochlear epithelium and employed the "Point selections" tool in Image J to count the number of immunostaining-positive cells. Quantification of cells/0.1 mm was calculated as total immunostaining positive cell number/total length of the epithelia (μm) × 100.

Statistical analysis

The mean ± SD represents all data, with each experiment conducted a minimum of three times. Statistical analyses utilized Microsoft Excel (2016, Microsoft Corporation, China) and SPSS 27 (27.0.1.0, IBM, United States) software, employing a one-way ANOVA followed by Dunnett's multiple comparisons test for comparisons involving more than two groups. Data were tested for normality using the Shapiro-Wilk tests in the statistical descriptive tools in SPSS. The homogeneity of variance test was performed using Levene's tests in the compare means tool. The Kruskal-Wallis H-test was used instead of one-way ANOVA when the data did not conform to normality. Welch's ANOVA was used to analyze the data when it did not conform to homogeneity of variance. In a design with multiple experimental groups and a single control group, Dunnett's test becomes superior to Tukey's HSD and Bonferroni correction through precise control of Type I errors and high statistical efficacy. A P value < 0.05 indicated statistical significance.

Ethical statement

The research protocol was evaluated and authorized through the Animal Protection Committee of the Shandong Provincial Hospital affiliated with Shandong First Medical University (Approval No. ECAESDUSM 20123011).

RESULTS

PJ34 protects HEI-OC1 cells and HCs from cisplatin-induced cellular damage

Flow cytometry analysis demonstrated a marked elevation in apoptotic index within the 30 μM cisplatin group (F (4,10) =158.3, 6.10±0.41 for Control, P<0.001). In the PJ34 plus cisplatin group, the apoptosis rate was significantly reduced at a concentration of 2.5 μM of PJ34 (0.41±0.02 for Cisplatin, P<0.001). As the concentration of PJ34 increased, the apoptosis rate gradually increased, indicating that the cisplatin-induced apoptosis of HEI-OC1 cells could be minimized at a concentration of 2.5 μM of PJ34 (Fig. 1 A and B). Immunofluorescence findings displayed that HCs in the cisplatin

group exhibited extensive degeneration and anatomical changes, such as cell plasma atrophy, structural disorders, as well as a large number of HCs detachment ($F(4,10)=59.57$, 0.36±0.04 for Control, $P<0.001$). The PJ34 plus cisplatin group showed more surviving HCs with fewer morphological alterations and better alignment than the cisplatin group. When PJ34 was present at 2.5 μM, the number of surviving HCs was the highest, and four rows of HCs were structurally more complete (2.64±0.34 for Cisplatin, $P<0.001$). When the concentration was 5 μM, the HCs were partially missing, and the cells were arranged slightly loosely (1.91±0.21 for Cisplatin, $P<0.001$). When the concentration was increased to 10 μM, the outer HCs were missing more severely, the inner HCs showed morphological changes, and the cell arrangement was slightly disorganized (1.57±0.11 for Cisplatin, $P<0.01$) (Fig. 1 C). Cell counts showed that there was a marked reduced in the number of surviving HCs in the cisplatin group, which was attenuated by the PJ34 co-treatment, particularly in the subgroup treated with a concentration of PJ34 at 2.5 μM (Fig. 1 D). According to these findings, we chose 2.5 μM PJ34 as the optimum concentration for follow-up experiments.

PJ34 promotes apoptosis in cisplatin-treated ovarian cancer cell lines

Flow cytometry results showed that treatment of HEY cell lines with 30 μM cisplatin resulted in a remarkable rise in apoptosis than control (F (4,10)2, 9.25±2.14 for Control, $P<0.01$). Additionally, when cisplatin was co-treated with different concentrations of PJ34, the apoptosis rate was higher than that of the group not treated with PJ34 (1.19±0.06, $P>0.05$ for 2.5 μM+ Cisplatin, 1.59±0.49, $P<0.01$ for 5 μM+ Cisplatin, 1.70±0.45, $P<0.01$for 10 μM+ Cisplatin). Furthermore, the apoptosis rate was positively associated with PJ34 concentration (Fig. 2 A and C). In TOV112D cell lines, the apoptotic rate was slightly higher after 30 μM cisplatin treatment than the control. However, this difference was not statistically significant ($F(4,10)=2.518$, 1.62±0.13 for Control, $P>0.05$). Treatment with 2.5 μM and 5 μM PJ34 had a slight effect on the apoptotic rate caused by cisplatin, but when the concentration of PJ34 was increased to 10 μM, the apoptosis rate was markedly increased. This increase was statistically

significant with respect to controls (21.48±11.67 for Control, $P<0.05$) (Fig. 2 B and D). In general, PJ34 enhanced the killing effect of cisplatin on TOV112D and HEY cell lines, however, in different cell lines, the effect of the same concentration of PJ34 on cisplatin-induced apoptosis was differential.

PJ34 alleviates cell death following cisplatin action in a caspase-independent manner

Immunofluorescence showed strong positivity for cleaved caspase-3 fluorescence in both HEI-OC1 cells and HCs, either in the cisplatin group or in the PJ34 plus cisplatin group (Fig. 3 A and C). Analysis of the mean fluorescence intensity of cleaved caspase-3 showed that the difference between the two treatment groups was not statistically significant ($F(2, 6) = 53.75$, 0.87±0.09, $P>0.05$ for Cisplatin in HEI-OC1 cells, $F(2, 6) = 21.12$, 1.02±0.05, $P>0.05$ for Cisplatin in HCs) (Fig. 3 B and D). The WB results indicated a marked elevation in cleaved caspase-3 protein expression levels in both the cisplatin group ($F(2, 6) = 55.44$, 27.87±18.28 for Control, $P<0.001$) and the PJ34 plus cisplatin group (23.97±11.05 for Control, $P<0.001$) with respect to the controls. Nonetheless, the difference between the two treatment groups was not statistically significant (0.89±0.07 for Cisplatin, $P<0.05$) (Fig. 3 E and F). In short, findings from both immunofluorescence and WB analyses indicated that PJ34 had no impact on the level of cleaved caspase-3 after cisplatin action.

PJ34 attenuated PARP-1 hyperactivation after cisplatin exposure

Immunofluorescence results showed that the fluorescence intensity of PARP-1 was stronger in the cisplatin group than in the controls ($F(2, 6) = 10.34$, 7.05±7.76 for Control, $P<0.01$), while PJ34 co-treatment reduced the fluorescence intensity of PARP-1 (0.51±0.19 for Cisplatin, $P<0.05$) (Fig. 4 A and B). WB results confirmed that the PARP-1 protein level was reduced in the PJ34 plus cisplatin group compared to the cisplatin group ($F(2, 6) = 10.63$, 0.84±0.10 for Cisplatin, $P<0.05$) (Fig. 4 C and D).

Cisplatin induced cell death by inducing AIF into the nucleus in a caspase-independent manner, which was attenuated by PJ34 co-treatment

Immunofluorescence staining of HCs displayed that in controls (Fig. 5A), AIF was detected mainly in the cytoplasmic region of HCs (yellow arrows), and the red fluorescence of AIF was almost absent in the nucleus. In the cisplatin group, the cytoplasm of HCs was wrinkled and some of the fluorescence of AIF appeared in the nucleus (yellow arrow). PJ34 co-treatment attenuated cytoplasmic morphological alterations, AIF was mostly expressed in the cytosol (yellow arrow), and PJ34 alleviated nuclear translocation of AIF. Co-localization analysis showed that PJ34 attenuated cisplatin-induced nuclear translocation of AIF. Immunofluorescence of the HEI-OC1 cell line showed similar results (Fig. 5C, yellow arrows). In addition, nucleoplasmic separation of HEI-OC1 cells demonstrated increased AIF expression in the nucleus in the cisplatin group ($F(2, 6)=255.4$, 1.20±0.008 for Control, $P<0.001$), whereas PJ34 decreased the tendency of AIF to enter the nucleus（0.90±0.02 for Cisplatin, $P<0.001$) (Fig. 5 E and F).

PJ34 alleviated cisplatin-induced reduction of MMP and accumulation of mitochondrial ROS in HEI-OC1 and HCs

MitoSOX Red staining showed strong positivity after cisplatin action ($F(2, 6)=21.14$, 2.02±0.49, $P< 0.001$ for Control in HEI-OC1 cells, $F(2, 6)=40.06$, 5.88±1.44, $P<0.001$ for Ctrl in HCs) and weaker positivity in the PJ34 plus cisplatin group (0.64±0.06, $P<0.01$ for Cisplatin in HEI-OC1 cells, 0.22±0.05, $P< 0.001$ for Cisplatin in HCs) in both HEI-OC1 cells and HCs (Fig. 5C-F). MMP assay exhibited a decrease in MMP due to cisplatin exposure compared to normal controls ($F (2, 6) =622.2$, 2.70±0.05 for Control, $P<0.001$). Co-treatment with PJ34 alleviated the extent of MMP decline (0.58±0.03 for Cisplatin, $P<0.001$) (Fig. 6 A and B). These observations demonstrate that in cochlear hair cells, cisplatin injury can lead to an elevation of mitochondrial ROS and a decrease in MMP, whereas PJ34 co-treatment attenuates these trends.

DISCUSSION

In our current investigation, immunofluorescence staining demonstrated that cochlear basement membrane exposed to cisplatin displayed considerable loss of cells, along with morphological alterations and structural disorganization. The histologic alterations in cisplatin-induced hearing loss are in agreement with our prior study [19]. The results of flow cytometry and immunofluorescence showed that 2.5 μM PJ34 effectively reduced cisplatin-induced HEI-OC1 cell death. Then, we explored the influence of PJ34 on the anti-ovarian cancer effects of cisplatin. The outcomes exhibited an increase in apoptosis in all PJ34 co-treated cells versus the cisplatin group, suggesting that PARPi increases the vulnerability of ovarian cancer cells to cisplatin, which is consistent with previous findings [10, 28]. Subsequently, we delved into understanding how PJ34 mitigates cisplatin-induced cellular damage. Our observations in the present study showed an increase in cleaved Caspase-3 levels after cisplatin treatment. This demonstrates cisplatin initiates apoptosis mainly through the mitochondrial apoptotic pathway, which is in accordance with our previous study [26, 28]. We observed no significant alteration in cleaved caspase-3 expression with co-treatment of PJ34, indicating that PJ34 mitigated cisplatin-induced cell death in a caspase-independent manner. Previous reports have highlighted parthanatos as a novel identified death pathway of cochlear HCs, mediating noise-induced hearing loss [29, 30]. Thus, we postulated that parthanatos exert an important function in the mechanism by which PJ34 attenuates cisplatin-induced ototoxicity. However, as both apoptosis and parthanatos involve the translocation of phosphatidylserine to the cell membrane surface, standard assay kits using only Annexin ν and propidium iodide staining cannot separate apoptosis from parapoptosis [31]. To address this challenge, we focused on the key parthanatos events, specifically the activation of PARP-1 and changes in the subcellular localization of AIF. Firstly, we investigated how cisplatin affects PARP-1 protein levels. The findings revealed an increase in PARP-1 protein expression following exposure to cisplatin. In contrast, PJ34 effectively attenuated the cisplatin-induced upregulation of

PARP-1. By pharmacologically inhibiting PARP-1 protein, we demonstrated that PARP-1 serves as a pivotal mediator of cisplatin-induced damage to HCs, with its activation closely associated with cisplatin-induced hearing loss. Inhibiting its expression could offer a promising strategy to mitigate cisplatin-induced ototoxicity. Secondly, we examined the expression differences of AIF in the nucleus and cytoplasm after cisplatin and PJ34 treatments. As a protein localized in mitochondria, its pro-apoptotic function is attributed to its nuclear translocation. However, there is uncertainty about the mechanism of PARP-1-dependent release of AIF in mitochondria, which may be related to factors such as PAR generation, disruption of MMP, or mitochondrial fission [32]. Our experimental results suggest that cisplatin promotes the movement of AIF from the cytoplasm into the nucleus, where AIF collaborates with the caspase-dependent pathway to induce cell death. Co-treatment with PJ34 reduced AIF levels in the nucleus and attenuated cisplatin-induced cellular damage. Building on these findings, we considered that PARP-1- and AIF-mediated parafoveal hearing loss exerts an essential role in cisplatin-induced hearing impairment. Furthermore, rescuing cells from parthanatos dependent cell death may represent a key mechanism underlying the hearing-protective effects of PJ34. Finally, since parthanatos is closely associated with mitochondrial dysfunction, we explored and the changes in ROS levels and MMP after cisplatin treatment. MitoSOX staining showed that exposure to cisplatin increased mitochondrial ROS accumulation, whereas MMP assay displayed that cisplatin evoked a loss of MMP. These findings suggest that cisplatin-induced accumulation of ROS and the reduction of MMP are important causes of cochlear hair cell injury. In addition, PJ34 co-treatment attenuated the increase in ROS levels and the decrease in MMP, suggesting that PJ34 may attenuate cisplatin-induced ototoxicity by alleviating mitochondrial dysfunction.

Notably, when exploring the optimal concentration of PJ34 to attenuate cisplatin-induced damage in auditory cells, we found that its function of attenuating cisplatin-induced cell death was gradually weakened with the increase in the concentration of

PJ34, suggesting that there is a strict concentration limitation for PJ34 to exert the effect of attenuating cisplatin-induced ototoxicity, and that a high concentration of PJ34 may be detrimental to its protective effect on cochlear hair cells. As a DNA repair inhibitor, high PJ34 doses may lead to exacerbated cellular DNA damage and increased apoptosis. Ensuring maximization of PARP-1 inhibition while minimizing potential toxicity is a key point of the study. Indeed, low doses of PJ34 were sufficiently protective in other non-tumor pathology models[6, 33]. Therefore, based on safety and efficacy considerations, we prioritized its lower dose range when selecting the concentration of action in the pre-experimental phase. Overall, One plausible interpretation of these results is that there may be a dose-dependent inhibitory effect of PJ34 on damaged DNA repair in the cochlea. This could lead to an imbalance between the cellular DNA break and repair system when the intracellular accumulation of PJ34 reaches a certain threshold, and that even a high concentration of PJ34 may aggravate cisplatin-induced hair cell damage. Actually, due to the existence of blood-labyrinth barrier (BLB) in the inner ear, a functional barrier consisting of tightly connected non-porous capillaries, makes the rate of drug transfer from the blood into the inner ear reduced [34]. When high doses of PJ34 are used as an anticancer drug, the levels of the drug in the cochlea may be much lower than that in the blood, avoiding the high concentration of PJ34 injury to HCs. This suggests that special attention should be given to accurately determining of dose-effect curves when using different drug combinations to exert synergistic effects, and that the concentration of PJ34 should be strictly monitored to optimize the combined effects of the drugs. Although this study discovered that low concentrations of PJ34 exhibited resistance to cisplatin ototoxicity, the exact mechanism causing varied cumulative effects at different concentrations remains unclear, necessitating further research. Another possible explanation is the off-target effect of high concentrations of PJ34. Madison et al. reported that high micromolar concentrations of PJ34 induce mitotic arrest in cancer cell lines and fibroblasts, independent of PARP-1/2. Antolín et al. noted that PJ34 interacts with multiple targets, including Pim1, which may contribute to cell cycle arrest at concentrations above 5 μM

[35, 36]. In summary, the confounding effects of targets such as Pim1 should be taken into account when using PJ34. Co-treatment with cisplatin using 2.5 μM, 5 μM, or 10 μM of PJ34 showed a clear disparity in cell survival, although all of these concentrations attenuated cisplatin-induced damage to mouse cochlear hair cells. This suggests that there may be an inflection point in the concentration interval of 2.5 to 5 μM where PJ34 most efficiently exerts both its role in attenuating cisplatin-induced ototoxicity and where it produces PARP-1-independent effects. To address this critical issue, it was required to specifically inhibit Pim targets in HEI-OC1 cells and HCs to explore their relationship with cell growth inhibition, and try to find effective ways to mitigate the off-target effects of PJ34. In addition, another interesting point is that we found that the effect of PJ34 in enhancing the anticancer effect of cisplatin was not significant in the TOV112D cell lines. In response to this result, we speculate that a possible explanation is that the PJ34 treatment concentration or time we set is not the optimum for it to exert cisplatin sensitization in the TOV112D cell lines. Another possible explanation is that the concentration of 30 μM cisplatin may not be optimal for its antitumor effects. This is evident from the marginal increase in the apoptotic rate when cisplatin is used alone. In contrast, the synergistic effect of PJ34 in enhancing cellular sensitivity to cisplatin may necessitate a sufficient concentration of cisplatin to induce DNA damage. In addition, it has been shown that cisplatin resistance may be associated with a particular situation in which a genetic mutation or epigenetic alteration in the TOV112D cell line results in the reactivation of BRCA1/2, which leads to the reestablishment of homologous homologous recombination repair (HRR) [37]. Also, activation of non-homologous end-joining or other alternative repair pathways that bypass PARPi-mediated inhibition of DNA repair is an important mechanism of resistance [38]. The specific mechanisms underlying this phenomenon require further research in the future.

In the present study, in addition to demonstrating that PJ34 could protect against cellular damage after cisplatin exposure via inhibition of PARP-1-AIF-mediated

parthanatos and attenuation of mitochondrial dysfunction, we also confirmed the antitumor effect of PJ34. Since PARPi were first reported to be used in the clinic as monotherapies for the treatment of cancers with mutations in the BRCA gene, they have been widely used, often as stand-alone anticancer drugs or in conjunction with additional platinum-based drugs for the treaurement of tumors including ovarian and breast cancers [39]. In this research, we demonstrated for an initial time that PJ34 attenuates cisplatin-induced damage to HEI-OC1 cells and HCs without destroying cisplatin's antitumor efficacy, which is the greatest innovation and value of this experiment compared with other studies. Indeed, a key issue that must be considered in the study of cisplatin otoprotective agents is whether the intervention affects the pharmacological effects of cisplatin's anticancer action, and a number of drugs thought to reduce cisplatin-induced damage to auditory cells have been found to potentially interfere with cisplatin's antitumor efficacy [40]. The anticisplatin ototoxicity as well as anticancer effects of PJ34 confirmed in the present study and the great potential of PJ34 against cisplatin nephrotoxicity reported in other studies make PJ34 stand out as one of the most promising candidates among the many otoprotective drugs, which would be a great achievement in the field of audiology.

However, there are some limitations to this study. To begin with, according to the experimental results, we found that cisplatin treatment for 24 hours resulted in elevated ROS and PARP-1 activation. However, due to the limited test duration of 24 hours, we were unable to determine the upstream-downstream relationship between these two events. Actually, it has been suggested that ROS accumulation is strongly related to PARP-1 overexpression. Mechanistically, ROS accumulation activates PARP-1 overexpression, which in turn promotes further ROS production. The mutually reinforcing effect between ROS and PARP-1 ultimately promotes PARP-1-mediated parthanatos[3]. Whether such a relationship exists in cisplatin-induced auditory cell damage requires further investigation in future studies. Secondly, in the current research, we proved that PJ34 attenuated ROS accumulation and the decrease in MMP after

cisplatin treatment, but the relationship between ROS generation and MMP has not yet been explored. The relationship between ROS accumulation and AIF nucleocytoplasmic relocalization remains unclear. While most studies suggest ROS promotes AIF translocation via mitochondrial damage (e.g., membrane potential loss, permeability pore opening, and calcium overload) [41-43], this conclusion largely relies on ROS scavengers like NAC. Future studies using specific AIF translocation inhibitors may clarify this mechanism. Additionally, how PJ34-mediated reduction in DNA damage attenuates AIF translocation is uncertain. Although AIF translocation is linked to DNA fragmentation [44, 45], severe DNA damage may overactivate PARP-1, further enhancing AIF nuclear translocation-a mechanism requiring further investigation. However, our study was limited to assessing PJ34 and cisplatin effects in HEI-OC1 cells and P3 mice cochlear explants. This experiment is an in vitro study on cochlear hair cells and culture of cochlear basilar membrane tissues from P3 mice. As it lacks validation through in vivo experiments on adult mice, the study has certain limitations and remains at the theoretical level. Performing in vivo experimental validation in the next step is our plan to move closer to clinical practical application.

CONCLUSION

In summary, the results of the current study demonstrate that cisplatin may induce the death of HEI-OC1 cells and HCs through caspase-dependent and caspase-independent pathways. In addition, PJ34 confers protective effects on cochlear hair cells against cisplatin-induced damage by suppressing parthanatos. Crucially, PJ34 may offer a practicable otoprotective strategy for patients receiving cisplatin. This discovery is particularly exciting given the severe ototoxicity associated with cisplatin, and PJ34 holds great promise for use in coalition with platinum-based agents in the therapy of a variety of malignant tumors. Further studies are needed to obtain an understanding of the specific mechanisms by which PJ34 resists cisplatin-induced ototoxicity.

Conflicts of interest: Authors declare no conflicts of interest.

Funding: This work was supported by the National Science Fund for Distinguished Young Scholars, China, 82201293

Data availability statement: The data that support the findings of this study are openly available in Mendeley Data at https://data.mendeley.com/datasets/zxzgp65bx5/1. All other data presented are contained within the manuscript/supplemental data.

Submitted: 12 April 2025

Accepted: 10 June 2025

Published online: 20 June 2025

REFERENCES

1. Vitali R, Mancuso AB, Palone F, *et al.* PARP1 activation induces HMGB1 secretion promoting intestinal inflammation in mice and human intestinal organoids. **Int J Mol Sci**. 2023;24(8):7096. doi:10.3390/ijms24087096
2. Konecny GE, Kristeleit RS. PARP inhibitors for BRCA1/2-mutated and sporadic ovarian cancer: current practice and future directions. **Br J Cancer**. 2016;115(10):1157-1173. doi:10.1038/bjc.2016.311
3. Chiu LY, Ho FM, Shiah SG, *et al.* Oxidative stress initiates DNA damage: MNNG-induced poly(ADP-ribose) polymerase-1-dependent parthanatos cell death. **Biochem Pharmacol**. 2011;81(3):459-470. doi:10.1016/j.bcp.2010.10.016
4. Jiang D, Yang X, Ge M, *et al.* Zinc defends against parthanatos and promotes functional recovery after spinal cord injury through SIRT3-mediated antioxidative stress and mitophagy. **CNS Neurosci Ther**. 2023;29(10):2857-2872. doi:10.1111/cns.14222
5. Huang S, Zhang B, Chen Y, *et al.* Poly(ADP-ribose) polymerase inhibitor PJ34 attenuated hepatic triglyceride accumulation in alcoholic fatty liver disease in

mice. **J Pharmacol Exp Ther**. 2018;364(3):452-461. doi:10.1124/jpet.117.243105

6. Zha S, Li Z, Cao Q, *et al.* PARP1 inhibitor (PJ34) improves the function of ageing-induced endothelial progenitor cells by preserving intracellular NAD^+ levels and increasing SIRT1 activity. **Stem Cell Res Ther**. 2018;9:186. doi:10.1186/s13287-018-0961-7
7. Hatachi G, Tsuchiya T, Miyazaki T, *et al.* The poly(ADP-ribose) polymerase inhibitor PJ34 reduces pulmonary ischemia-reperfusion injury in rats. **Transplantation**. 2014;98(6):618-624. doi:10.1097/TP.0000000000000305
8. Mascolo M, Ilardi G, Romano MF, *et al.* Over-expression of chromatin assembly factor-1 p60, poly(ADP-ribose) polymerase-1 and nestin predicts metastasising behaviour of oral cancer. **Histopathology**. 2012;61(6):1089-1105. doi:10.1111/j.1365-2559.2012.04313.x
9. Gadad SS, Camacho CV, Malladi V, *et al.* PARP-1 regulates oestrogen-dependent gene expression in oestrogen receptor-α-positive breast cancer cells. **Mol Cancer Res**. 2021;19(10):1688-1698. doi:10.1158/1541-7786.MCR-21-0103
10. Cheng H, Zhang Z, Borczuk A, *et al.* PARP inhibition selectively increases sensitivity to cisplatin in ERCC1-low non-small-cell lung cancer cells. **Carcinogenesis**. 2013;34(4):739-749. doi:10.1093/carcin/bgs393
11. Olaussen KA, Adam J, Vanhecke E, *et al.* PARP1 impact on DNA repair of platinum adducts: preclinical and clinical read-outs. **Lung Cancer**. 2013;80(2):216-222. doi:10.1016/j.lungcan.2013.01.014
12. Hastak K, Alli E, Ford JM. Synergistic chemosensitivity of triple-negative breast-cancer cell lines to poly(ADP-ribose) polymerase inhibition, gemcitabine and cisplatin. **Cancer Res**. 2010;70(20):7970-7980. doi:10.1158/0008-5472.CAN-09-4521

13. Mukhopadhyay P, Horváth B, Kechrid M, *et al.* Poly(ADP-ribose) polymerase-1 is a key mediator of cisplatin-induced kidney inflammation and injury. **Free Radic Biol Med**. 2011;51(9):1774-1788. doi:10.1016/j.freeradbiomed.2011.08.006
14. Kim MJ, Moon D, Jung S, *et al.* Cisplatin nephrotoxicity is induced via poly(ADP-ribose) polymerase activation in adult zebrafish and mice. **Am J Physiol Regul Integr Comp Physiol**. 2020;318(5):R843-R854. doi:10.1152/ajpregu.00130.2019
15. Kim HJ, Oh GS, Shen A, *et al.* Augmentation of NAD^+ by NQO1 attenuates cisplatin-mediated hearing impairment. **Cell Death Dis**. 2014;5:e1292. doi:10.1038/cddis.2014.255
16. Cai J, Wu X, Li X, *et al.* Allicin protects against cisplatin-induced stria vascularis damage: possible relation to inhibition of caspase-3 and PARP-1-AIF-mediated apoptotic pathways. **ORL J Otorhinolaryngol Relat Spec**. 2019;81(4):202-214. doi:10.1159/000500557
17. Song Y, Fan Z, Bai X, *et al.* PARP-1-modulated AIF translocation is involved in streptomycin-induced cochlear hair-cell death. **Acta Otolaryngol**. 2016;136(6):545-550. doi:10.3109/00016489.2016.1143968
18. Kim SY, Lee JE, Kang SH, *et al.* The protective effects of human embryonic stem-cell-derived mesenchymal stem cells in noise-induced hearing loss of rats. **Cells**. 2022;11(21):3524. doi:10.3390/cells11213524
19. Zhang W, Man R, Yu X, *et al.* Hydroxytyrosol enhances cisplatin-induced ototoxicity: possible relation to alteration in JNK and AIF pathways. **Eur J Pharmacol**. 2020;887:173338. doi:10.1016/j.ejphar.2020.173338
20. Pushpan CK, Kresock DF, Ingersoll MA, *et al.* Repurposing AZD5438 and dabrafenib for cisplatin-induced AKI. **J Am Soc Nephrol**. 2024;35(1):22-40. doi:10.1681/ASN.0000000000000261

21. Wang X, Zhou Y, Wang D, *et al.* Cisplatin-induced ototoxicity: from signaling network to therapeutic targets. **Biomed Pharmacother**. 2023;157:114045. doi:10.1016/j.biopha.2022.114045
22. Rybak LP, Mukherjea D, Jajoo S, *et al.* siRNA-mediated knock-down of NOX3: therapy for hearing loss? **Cell Mol Life Sci**. 2012;69(14):2429-2434. doi:10.1007/s00018-012-1016-3
23. Li Y, Yang H, Nong H, *et al.* HMG-CoA reductase protects hair cells from cisplatin-induced ototoxicity *in vitro*: relation to p38 MAPK signaling. **Arch Toxicol**. 2023;97(11):2955-2967. doi:10.1007/s00204-023-03588-z
24. Herling AW. Euthanasia of experimental animals. In: Vogel HG, Maas J, Hock FJ, Mayer D, eds. **Drug Discovery and Evaluation: Pharmacological Assays**. 3rd ed. Springer; 2016:4277-4280. doi:10.1007/978-3-319-05392-9_134
25. Kumar M, Bansal PK. Euthanasia procedure used in experimental laboratory. In: **Animal Models of Neurological Disorders**. Springer; 2017:307-314. doi:10.1007/978-981-10-5981-0_20
26. Nong H, Song X, Li Y, *et al.* AdipoRon reduces cisplatin-induced ototoxicity in hair cells: relation to regulation of mitochondrial biogenesis. **Neurosci Lett**. 2024;819:137577. doi:10.1016/j.neulet.2023.137577
27. Schneider CA, Rasband WS, Eliceiri KW. NIH Image to ImageJ: 25 years of image analysis. **Nat Methods**. 2012;9(7):671-675. doi:10.1038/nmeth.2089
28. Zhao H, Xu Y, Song X, *et al.* Cisplatin induces damage of auditory cells: relation with dynamic variation in calcium homeostasis and responding channels. **Eur J Pharmacol**. 2022;914:174662. doi:10.1016/j.ejphar.2021.174662
29. Murashita H, Tabuchi K, Hoshino T, *et al.* Effects of tempol, 3-aminobenzamide and nitric-oxide synthase inhibitors on acoustic injury of the mouse cochlea. **Hear Res**. 2006;214(1-2):1-6. doi:10.1016/j.heares.2005.12.008

30. Marchetta P, Möhrle D, Eckert P, *et al.* Guanylyl cyclase A/cGMP signaling slows hidden, age- and acoustic-trauma-induced hearing loss. **Front Aging Neurosci**. 2020;12:83. doi:10.3389/fnagi.2020.00083
31. Maru B, Messikommer A, Huang L, *et al.* PARP-1 improves leukaemia outcomes by inducing parthanatos during chemotherapy. **Cell Rep Med**. 2023;4(9):101191. doi:10.1016/j.xcrm.2023.101191
32. Hong SJ, Dawson TM, Dawson VL. Nuclear and mitochondrial conversations in cell death: PARP-1 and AIF signaling. **Trends Pharmacol Sci**. 2004;25(5):259-264. doi:10.1016/j.tips.2004.03.005
33. Zha S, Wang F, Li Z, *et al.* PJ34, a PARP1 inhibitor, promotes endothelial repair in a rabbit model of high-fat-diet-induced atherosclerosis. **Cell Cycle**. 2019;18(17):2099-2109. doi:10.1080/15384101.2019.1640008
34. Nyberg S, Abbott NJ, Shi X, Steyger PS, Dabdoub A. Delivery of therapeutics to the inner ear: the challenge of the blood-labyrinth barrier. **Sci Transl Med**. 2019;11(482):eaao0935. doi:10.1126/scitranslmed.aao0935 pubmed.ncbi.nlm.nih.gov
35. Madison DL, Stauffer D, Lundblad JR. The PARP inhibitor PJ34 causes a PARP1-independent, p21-dependent mitotic arrest. **DNA Repair**. 2011;10(10):1003-1013. doi:10.1016/j.dnarep.2011.07.006
36. Antolín AA, Jalencas X, Yélamos J, Mestres J. Identification of Pim kinases as novel targets for PJ34 with confounding effects in PARP biology. **ACS Chem Biol**. 2012;7(12):1962-1967. doi:10.1021/cb300317y
37. Hong L, Wang X, Zheng L, *et al.* Tumour-associated macrophages promote cisplatin resistance in ovarian cancer cells by enhancing WTAP-mediated N^6-methyladenosine RNA methylation via the CXCL16/CXCR6 axis. **Cancer Chemother Pharmacol**. 2023;92(1):71-81. doi:10.1007/s00280-023-04533-8
38. Zeng S, Xu Z, Liu Y, *et al.* CRABP2 reduces the sensitivity of olaparib in ovarian cancer by down-regulating caspase-8 and decreasing reactive oxygen

species. **Chem Biol Interact**. 2024;393:110958. doi:10.1016/j.cbi.2024.110958

39. Moutafi M, Economopoulou P, Rimm D, Psyrri A. PARP inhibitors in head and neck cancer: molecular mechanisms, preclinical and clinical data. **Oral Oncol**. 2021;117:105292. doi:10.1016/j.oraloncology.2021.105292
40. Rybak LP, Alberts I, Patel S, *et al.* Effects of natural products on cisplatin ototoxicity and chemotherapeutic efficacy. **Expert Opin Drug Metab Toxicol**. 2023;19(9):635-652. doi:10.1080/17425255.2023.2260737
41. Kim BM, Choi YJ, Lee YH, *et al.* N,N-Dimethyl-phytosphingosine sensitises HL-60/MX2, a multidrug-resistant HL-60 variant, to doxorubicin-induced cytotoxicity through ROS-mediated release of cytochrome c and AIF. **Apoptosis**. 2010;15(8):982-993. doi:10.1007/s10495-010-0512-x
42. Xu L, Ma S, Qu M, *et al.* Parthanatos initiated by ROS-induced DNA damage is involved in intestinal epithelial injury during necrotising enterocolitis. **Cell Death Discov**. 2024;10(1):21. doi:10.1038/s41420-024-02114-z
43. Lee B, Qu Y, Wang S, *et al.* Newcastle disease virus infection induces parthanatos in tumour cells via calcium waves. **PLoS Pathog**. 2024;20(12):e1012737. doi:10.1371/journal.ppat.1012737
44. Wang Y, Kim NS, Haince J-F, *et al.* Poly(ADP-ribose) binding to apoptosis-inducing factor is critical for PARP-1-dependent cell death (parthanatos). **Sci Signal**. 2011;4(167):ra20. doi:10.1126/scisignal.2000902
45. Wang X, Li F, Liu J, *et al.* New insights into the mechanism of hepatocyte apoptosis induced by typical organophosphate ester: an integrated *in vitro* and *in silico* approach. **Ecotoxicol Environ Saf**. 2021;219:112342. doi:10.1016/j.ecoenv.2021.112342

FIGURES WITH LEGENDS

Figure 1

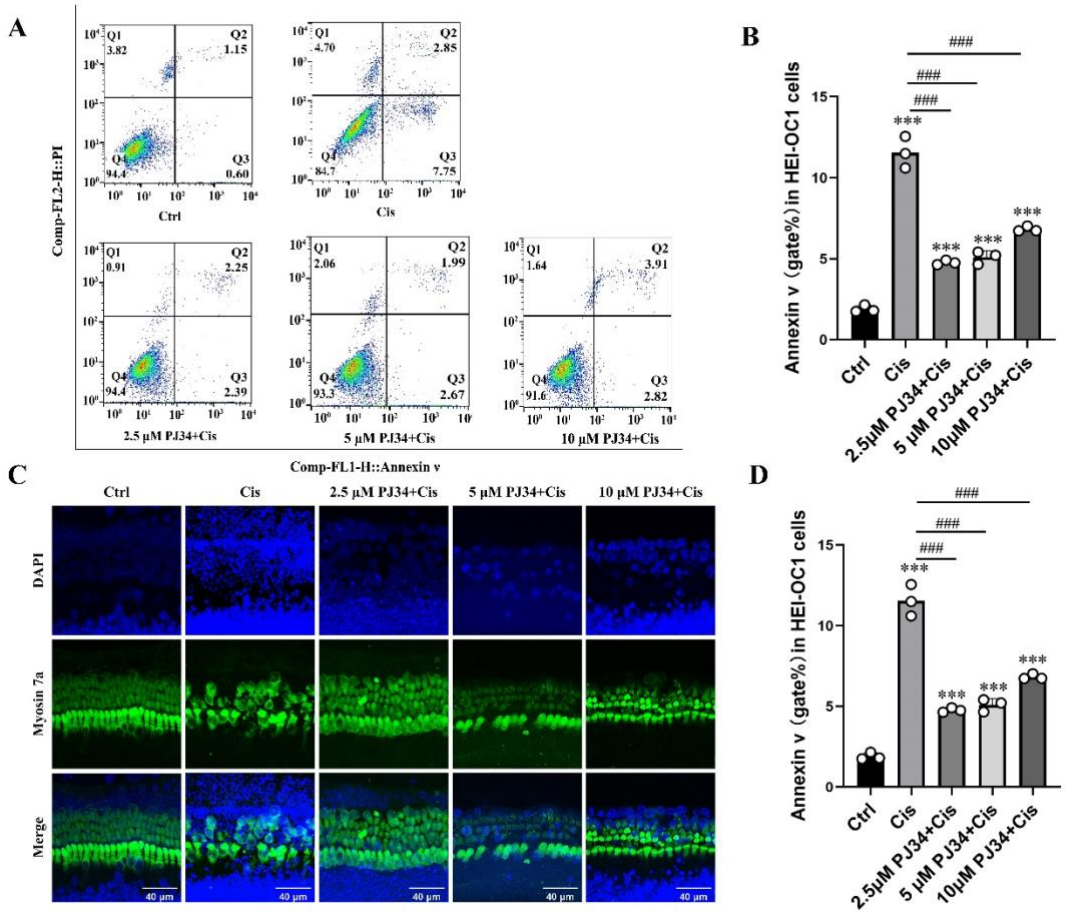

Figure 1. PJ34 ameliorated cisplatin-mediated injury to HEI-OC1 cells and HCs. (A) Flow cytometry shows the apoptotic rate of HEI-OC1 cells treated with different concentrations of PJ34 at 30 μM cisplatin. (B) Quantitative analysis of the results shown in (A). (C) Immunofluorescence staining shows the morphological changes induced by 30 μM cisplatin and different concentrations of PJ34 on HCs. Representative images of HCs labeled with Myosin 7a (green) and DAPI (blue) in different groups. (D) Quantification of Myosin 7a-positive HCs in different groups. *** $P < 0.001$ versus control group, ## $P < 0.01$ versus cisplatin group, ### $P < 0.001$ versus cisplatin group. n = 3. Scale bars = 40 μm.

Figure 2

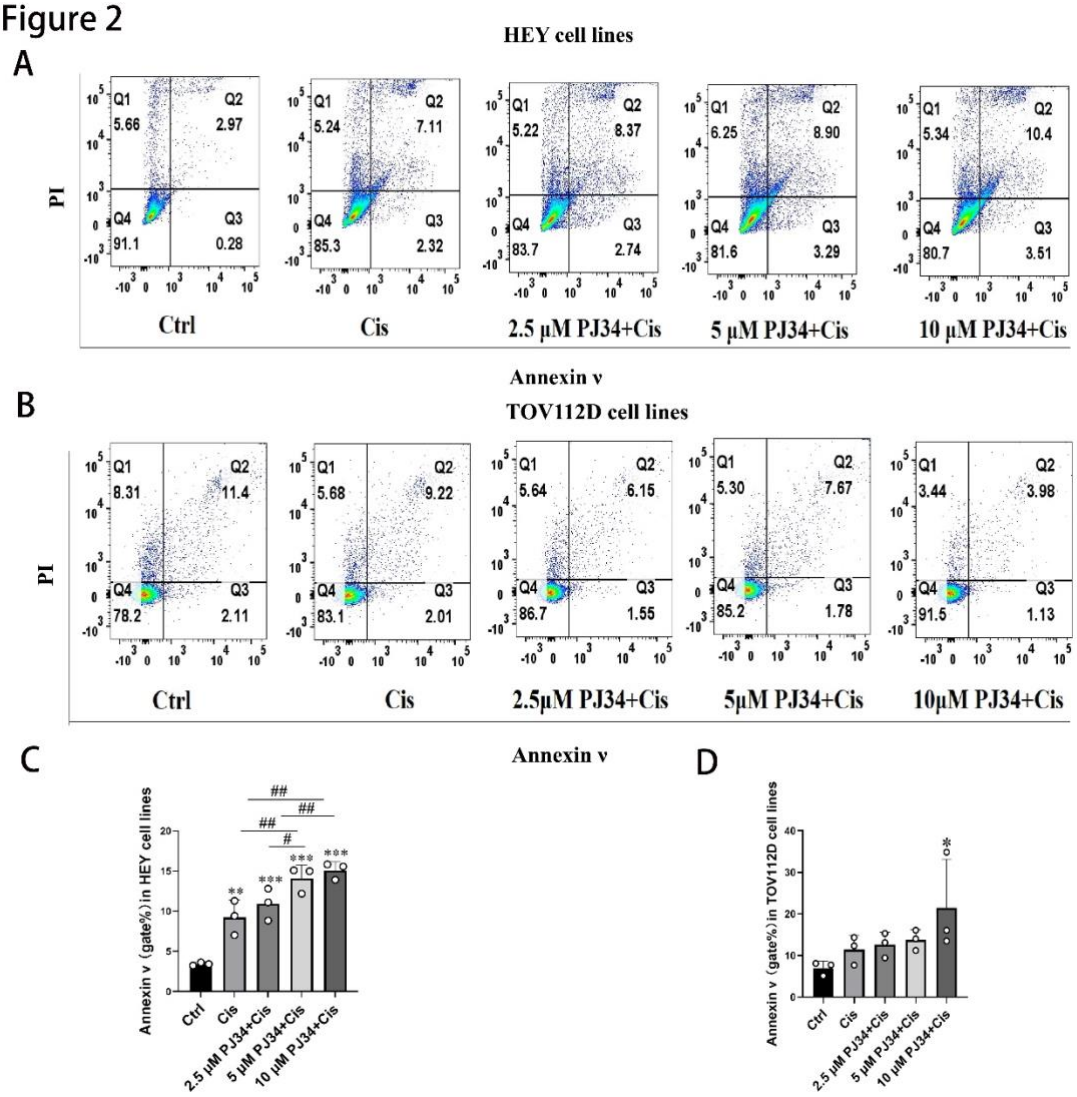

Figure 2. PJ34 aggravated cisplatin-induced cell death in HEY and TOV112D cell lines. (A and C) The apoptotic rate of HEY cell lines detected by flow cytometry and its quantitative analysis. (B and D) The apoptotic rate of TOV112D cell lines detected by flow cytometry and its quantitative analysis. * $P< 0.05$ versus control group, ** $P< 0.01$ versus control group, *** $P< 0.001$ versus control group, # $P< 0.05$ versus cisplatin group, ## $P< 0.01$ versus cisplatin group. A total of 10 000 cells were collected for each set of samples. n = 3

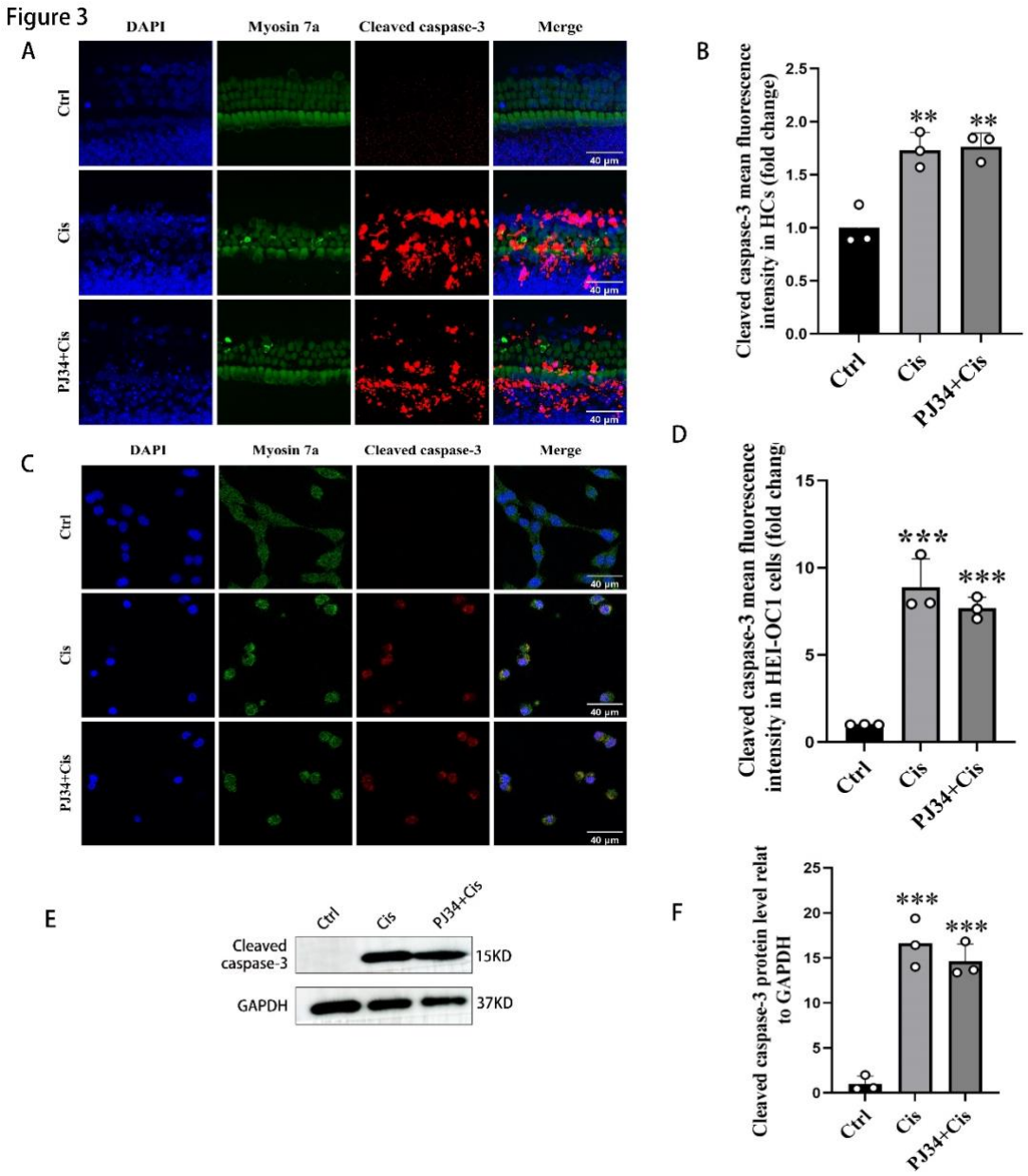

Figure 3. PJ34 attenuates cisplatin-induced cell death in HEI-OC1 cells and HCs via a caspase-3 independent pathway. (A) Double staining of cleaved caspase-3 (red) and Myosin 7a (green) in control, cisplatin and PJ34 plus cisplatin groups. (B) Quantitative analysis of cleaved caspase-3 shown in (A). The fluorescence intensity of cleaved caspase-3 was increased significantly after different treatments, but there was no difference in fluorescence intensity between the different treatments. (C) Immunofluorescence revealed the expression of cleaved caspase-3 in HEI-OC1 cells.

(D) Quantitative analysis of cleaved caspase-3 shown in (C). HEI-OC1 cells showed similar results to HCs. (E) Cleaved caspase-3 protein levels in HEI-OC1 cells from control, cisplatin and PJ34 plus cisplatin groups. GAPDH served as a loading control in each lane. (F) Quantitative analysis of proteins in (E). ** $P< 0.05$ versus control group, *** $P< 0.001$ versus control group. n = 3. Scale bars = 40 μm.

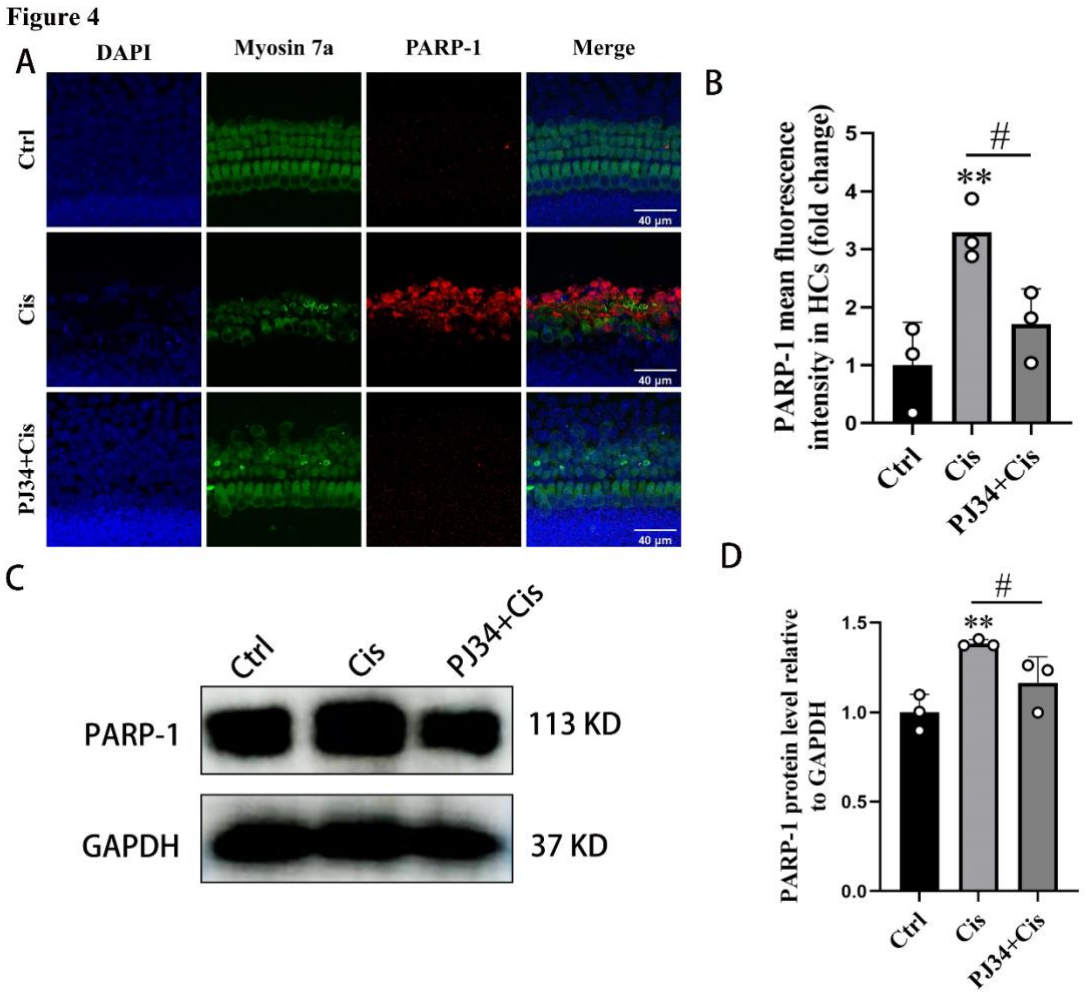

Figure 4. PJ34 attenuated cisplatin-activated PARP-1 levels. (A) Immunofluorescence shown changes in PARP-1 expression in different groups. (B) Quantitative analysis of the results presented in (A). （C）The dynamic changes of PARP-1 protein levels in HEI-OC1 cells after cisplatin exposure were detected by WB. (D) Quantitative analysis of the results presented in (C). * $P< 0.05$ versus control group, ** $P< 0.01$ versus control group, # $P< 0.05$ versus cisplatin group.

Figure 5

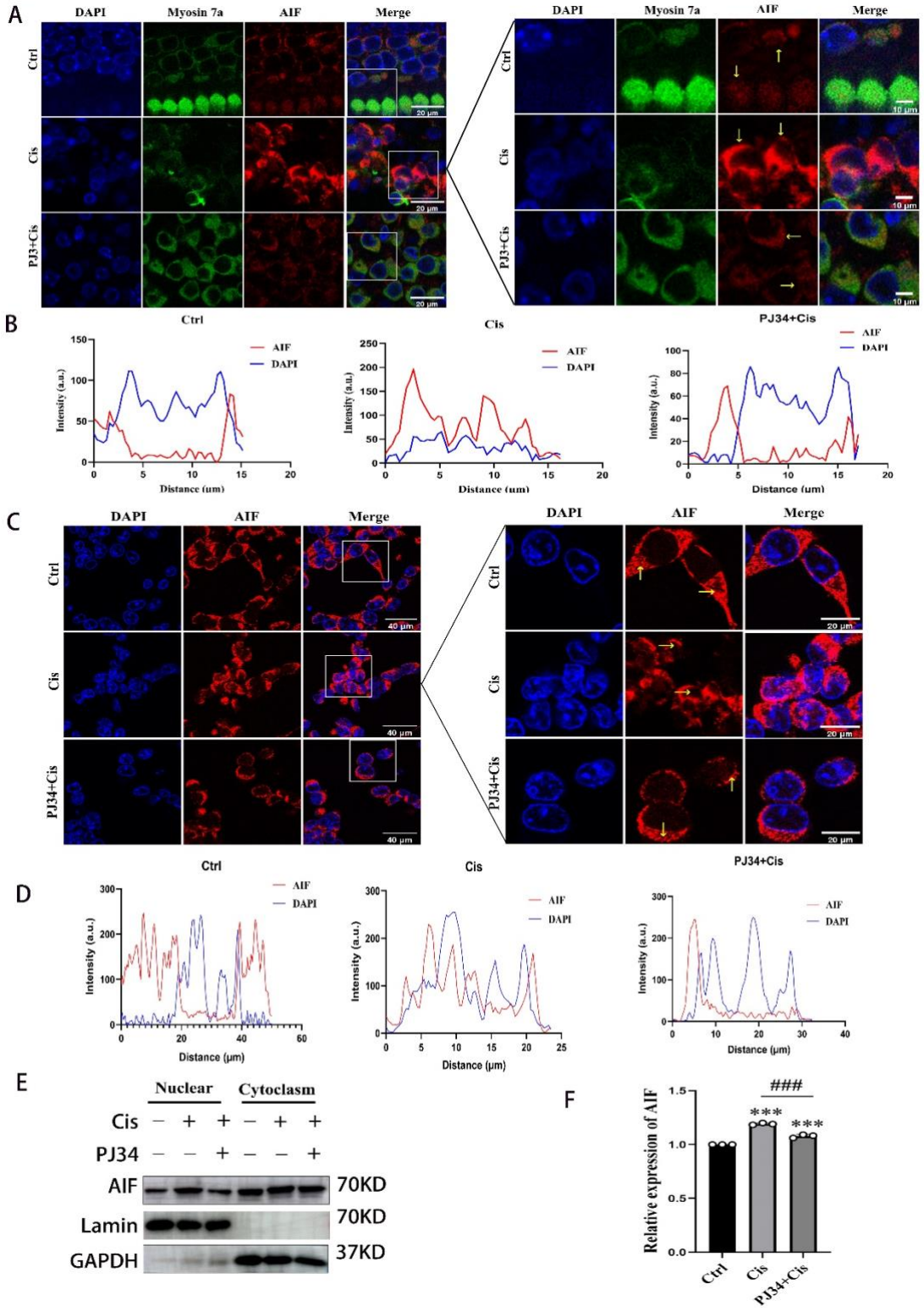

Figure 5. Cisplatin promoted nuclear translocation of AIF in HCs and HEI-OC1 cells, which was attenuated by PJ34. （A）AIF (red) and Myosin 7a (green) double

staining in control, cisplatin and PJ34 plus cisplatin group. The cytosol of HCs was labeled with Myosin 7a and the nucleus was labeled with DAPI (blue). (B) Co-location analysis of AIF and DAPI in A.（C）Differences in localization of AIF in HEI-OC1 cells after different treatments. (D) Co-location analysis of AIF and DAPI in C.（E）Cytoplasmic and nuclear proteins of HEI-OC1 cells were separated using a nucleoplasmic separation kit, and the lysates were detected by WB. Anti-lamin antibodies and anti-GAPDH antibodies were used to ensure equal loading of proteins of the nucleus and cytoplasm. （F）Quantitative analysis of the results presented in (E).

Figure 6

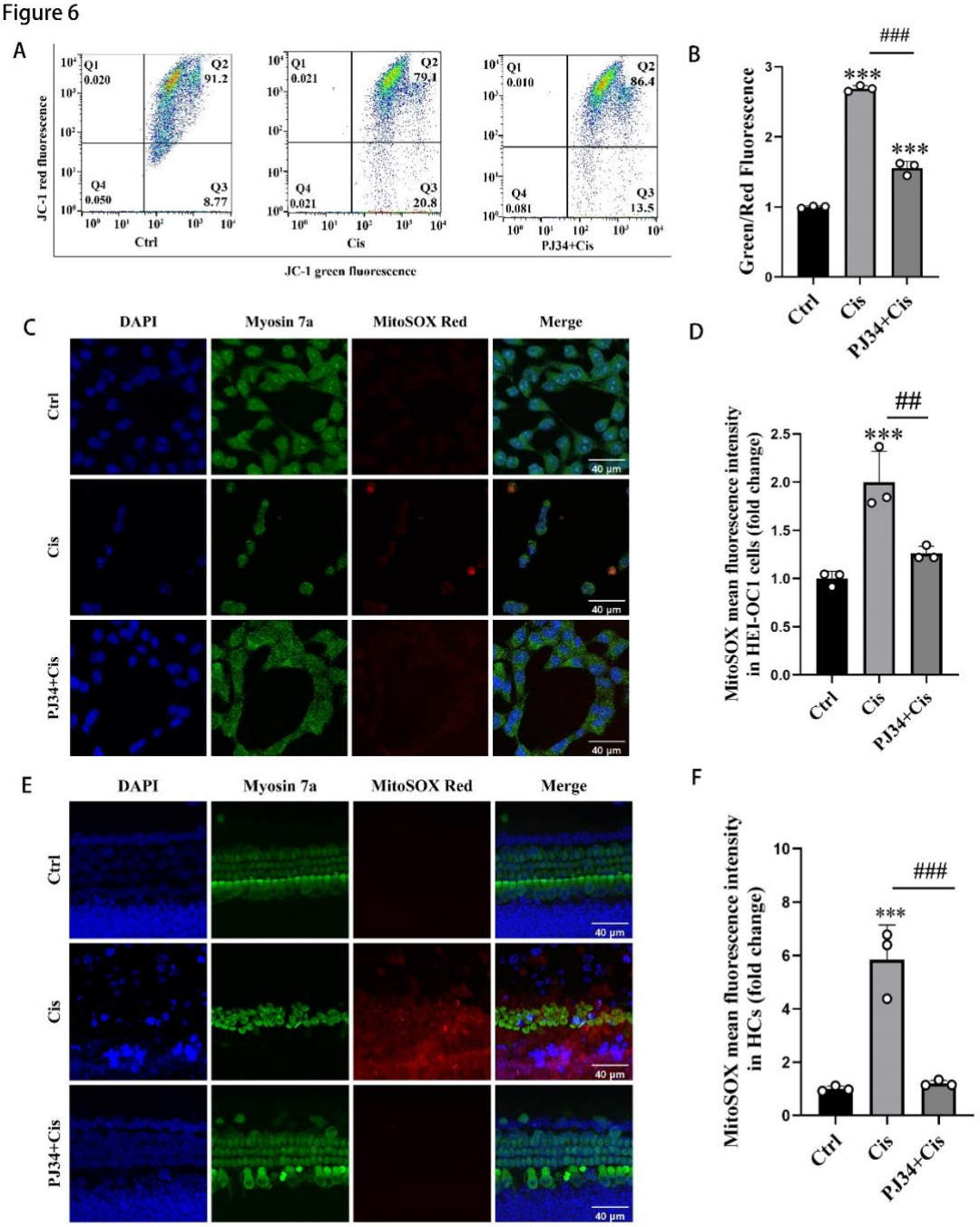

Figure 6. PJ34 attenuated the cisplatin-induced decrease in MMP and increase in mitochondrial ROS levels in HEI-OC1 cells and HCs. (A) The effects of cisplatin and PJ34 on the MMP of HEI-OC1 cells were detected by flow cytometry. (B) Quantitative analysis of the results presented in (A). (C) Representative images of MitoSOX staining (red) in the control, cisplatin and PJ34 plus cisplatin group. Myosin

7a (green) was used as the marker of HEI-OC1 cells. Scale bars = 40 μm. (D) Quantitative analysis of the results presented in (C). The data showed the mitochondrial ROS levels were decreased in PJ34 pretreated HEI-OC1 cells after cisplatin insult. (E) Mitochondrial ROS levels showed similar changes in HCs. (F) Quantitative analysis of the results presented in (E). *** $P< 0.001$ versus control group, ## $P< 0.01$ versus cisplatin group, ### $P< 0.001$ versus cisplatin group. n =3.